JBIC (1996) 1:117–126

ORIGINAL ARTICLE

L. Banci · I. Bertini · K.L. Bren · M.A. Cremonini
H.B. Gray · C. Luchinat · P. Turano

The use of pseudocontact shifts to refine solution structures of paramagnetic metalloproteins: Met80Ala cyano-cytochrome *c* as an example

Received: 11 July 1995 / Accepted: 30 October 1995

Abstract The availability of NOE constraints and of the relative solution structure of a paramagnetic protein permits the use of pseudocontact shifts as further structural constraints. We have developed a strategy based on: (1) determination of the χ tensor anisotropy parameters from the starting structure; (2) recalculation of a new structure by using NOE *and* pseudocontact shift constraints simultaneously; (3) redetermination of the χ tensor anisotropy parameters from the new structure, and so on until self-consistency. The system investigated is the cyanide derivative of a variant of the oxidized *Saccharomyces cerevisiae* iso-1-cytochrome *c* containing the Met80Ala mutation. The structure has been substantially refined. It is shown that the analysis of the deviation of the experimental pseudocontact shifts from those calculated using the starting structure may be unsound, as may the simple structure refinement based on the pseudocontact shift constraints only.

Key words Solution structure · Paramagnetic biomolecules · NMR · Cytochrome *c*

L. Banci · I. Bertini (✉) · P. Turano
Department of Chemistry, University of Florence,
Via G. Capponi 7, I-50121 Florence, Italy
Tel. +39-55-2757549; Fax +39-55-2757555;
e-mail bertini@risc1.lrm.fi.cnr.it

K.L. Bren · H.B. Gray
Arthur Amos Noyes Laboratory, California Institute of Technology, Pasadena, CA 91125, USA

M.A. Cremonini · C. Luchinat
Institute of Agricultural Chemistry, University of Bologna,
Viale Berti Pichat 10, I-40127 Bologna, Italy

Introduction

It is now possible to obtain dipolar connectivities through NMR in solution for paramagnetic metalloproteins [1–5]. Indeed, it has been recently shown that when the electron relaxation times are short enough, it is possible to detect NMR connectivities in the vicinity of a paramagnetic center and therefore to collect a sufficient number of NOE constraints to solve solution structures [6–12]. However, the presence of a paramagnetic center raises the threshold of detectability of NOE connectivities, and therefore the resolution of the structure around the metal ion may be lower than in other parts of the protein that are farther from the metal ion.

The pseudocontact part of the hyperfine coupling between unpaired electrons and resonating nuclei has long been utilized to obtain structural information in solution [13–17]. We show here that such structural constraints can be successfully employed in the determination of solution structures via NMR. Such constraints are particularly meaningful in the vicinity of the paramagnetic center and therefore may transform the disadvantage incurred by its presence into an advantage for a better solution structure.

The hyperfine coupling has a contact and a pseudocontact contribution [18–20]. The contact coupling is due to the presence of unpaired spin density on the resonating nucleus and vanishes a few chemical bonds away from the metal, unless π bonds are involved. The pseudocontact shifts arise from magnetic susceptibility anisotropy and depend on the nuclear position with respect to the principal axes of the magnetic susceptibility tensor:

$$\delta_i^{pc} = \frac{1}{12\,\pi r_i^3}\left[\Delta\chi_{ax}(3n_i^2-1)+\frac{3}{2}\Delta\chi_{rh}(l_i^2-m_i^2)\right] \qquad (1)$$

where $\Delta\chi_{ax}$ and $\Delta\chi_{rh}$ are the axial and the rhombic anisotropy of the magnetic susceptibility induced by the paramagnetic ion, r_i is the distance from the ion of an

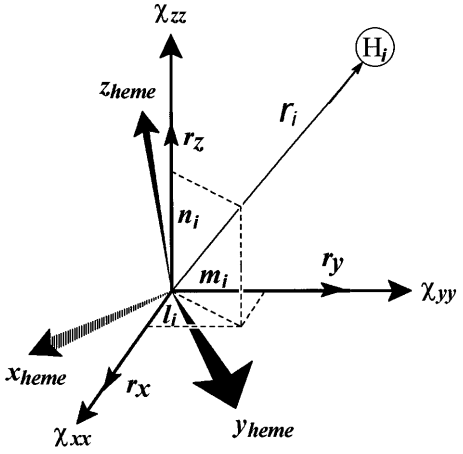

Fig. 1 The position of proton H_i with respect to the principal axes of the magnetic susceptibility tensor (χ_{xx}, χ_{yy}, χ_{zz}) can be expressed by the metal-proton distance, r_i, and by the direction cosines n_i, l_i, m_i of the vector $\mathbf{r_i}$ (Eq. 1). In a generic molecular reference frame x_{heme}, y_{heme}, z_{heme}, the same direction cosines can be expressed by the scalar products of $\boldsymbol{r_i}$ with the unit vectors $\boldsymbol{r_x}$, $\boldsymbol{r_y}$, $\boldsymbol{r_z}$ along χ_{xx}, χ_{yy}, χ_{zz} (Eq. 2). $\Delta\chi_{ax}$ and $\Delta\chi_{rh}$ in Eq. 2 are defined as: $\Delta\chi_{ax}=\chi_{zz}-\frac{1}{2}(\chi_{xx}+\chi_{yy})$ and $\Delta\chi_{rh}=\chi_{xx}-\chi_{yy}$

atom i, and l_i, m_i, and n_i are the direction cosines of the position vector of atom i ($\boldsymbol{r_i}$) with respect to the orthogonal reference system formed by the principal axes of the magnetic susceptibility tensor (Fig. 1).

If we know the hyperfine shifts, i.e. the differences in shift between the actual paramagnetic system and the analogous diamagnetic system, and if we can assume that the contact shift is zero, as is the case for all nuclei separated from the metal center by several chemical bonds, then we have the pseudocontact shift values, δ_i^{pc}. At this point, we may rely on a structure, e.g. that obtained through NOE constraints, to extract the polar coordinates for each proton with respect to an arbitrary internal axes frame and then find $\Delta\chi_{ax}$, $\Delta\chi_{rh}$, and the three independent direction cosines which define the principal directions of the χ tensor with respect to the above internal axes. This is the usual procedure to extract the magnetic susceptibility tensor anisotropy from the pseudocontact shifts and from a structural model [17, 21–25]. Recently, it has been proposed that an X-ray structure could be refined by varying the atomic coordinates in such a way as to minimize the deviation between experimental and calculated pseudocontact shifts [26].

Here we pursue the above idea by developing an algorithm to refine solution structures using *all* NMR constraints, including pseudocontact shifts, in a self-consistent fashion. Indeed, it is desirable to seek self-consistency among all experimental constraints (i.e. pseudocontact shifts and NOEs). If a structure is refined by using only pseudocontact shifts as constraints, larger disagreements with the experimental NOEs will be found and the refinement will not be reliable.

Materials and methods

The five parameters defining the magnetic susceptibility tensor anisotropy can be obtained by finding the best fit of Eq. 1 to a set of experimental δ_i^{pc} values. Iterative search or minimization procedures for this purpose have been reported by several authors [17, 21–23, 25, 27, 29]. We have written a program which relies on the well-known SIMPLEX [30] minimization algorithm [the program, called FANTASIA (Finding ANisotropy Tensors: A SImplex Approach) is available from the authors (m.a.cremonini@nmrlab.ciam.unibo.it) upon request]. The proton coordinates of an initial structure are then expressed in a Cartesian axes system centered on the paramagnetic center (the iron atom in this case) and defined with respect to a few atoms which are considered fixed in the structure. In the present case the z axis was defined as being perpendicular to the mean plane of the four heme nitrogens and positive on the histidine side; the x axis was taken along the projection on the mean plane of the metal-pyrrole III nitrogen bond; and the y axis, perpendicular to the former two in the direction of the pyrrole IV nitrogen.

The five parameters which define the χ tensor anisotropy with respect to any metal-centered axis system can then be determined by finding the best fit, to a set of δ_i^{pc} values, of Eq. 2, which is Eq. 1 rewritten in a more general form:

$$\delta_i^{pc}=\frac{1}{12\pi r_i^5}\left[\Delta\chi_{ax}(3(\boldsymbol{r_i}\cdot\boldsymbol{r_z})^2-r_i^2)+\frac{3}{2}\Delta\chi_{rh}((\boldsymbol{r_i}\cdot\boldsymbol{r_x})^2-(\boldsymbol{r_i}\cdot\boldsymbol{r_y})^2)\right] \quad (2)$$

where $\boldsymbol{r_i}$ are the position vectors of the protons relative to the chosen axis system and $\boldsymbol{r_x}$, $\boldsymbol{r_y}$, and $\boldsymbol{r_z}$ are unit vectors along the principal directions of the χ tensor (Fig. 1). The five parameters are $\Delta\chi_{ax}$, $\Delta\chi_{rh}$, and three independent direction cosines out of the nine direction cosines defining $\boldsymbol{r_x}$, $\boldsymbol{r_y}$, and $\boldsymbol{r_z}$ in the chosen axis system.

As a family of N NMR structures is usually available, an average tensor can be straightforwardly obtained by best-fitting, using the five χ tensor anisotropy parameters, an extended set of Eqs. 2 with N slightly different $\boldsymbol{r_i}$ vectors to the same experimental δ_i^{pc} values. In the case of methyl protons or fast-rotating ring protons, an average calculated δ_i^{pc} value is compared with the experimental one. The obtained χ tensor anisotropy parameters are then used in a modified version of the program DIANA [31, 32] (hereafter called PSEUDIANA) to recalculate δ_i^{pc} values after each change of structure, in order to add a contribution due to the pseudocontact shifts to the whole target function.

The program DIANA is based on the conjugate gradient algorithm [33, 34], which, in turn, relies (in this case) on the calculation of the gradient of the target function in the space of the dihedral angles [31, 32]. To implement the PSEUDIANA version, the contribution to the total target function, t^{tot}, introduced by the pseudocontact shift constraints, t^{pc}, has been defined as:

$$t^{pc}=k\sum_i[\max(|\delta_{i_{calc}}^{pc}-\delta_{i_{obs}}^{pc}|-T,0)]^2 \quad (3)$$

where the operator "max" yields the larger of the two values in parentheses separated by the comma, and T is the chosen tolerance (0.05 ppm in the present case). The k value that provides a proper weight of the δ_i^{pc} constraints with respect to the NOE constraints was estimated to be around 1 nm^2. In the present paper we used $k=1$ nm^2.

The contribution to the gradient was calculated as the first derivative of the pseudocontact target function, t_i^{pc}, with respect to the dihedral angles φ_j which affect an atom i:

$$\frac{\partial t_i^{pc}}{\partial\phi_j}=2k[\mathrm{sign}(\sqrt{t_i^{pc}},\delta_{i_{calc}}^{pc}-\delta_{i_{obs}}^{pc})]\frac{1}{12\pi r_i^5}\left[Q_x\left(\boldsymbol{r_x}\cdot\frac{\partial\boldsymbol{r_i}}{\partial\phi_j}\right)+Q_y\left(\boldsymbol{r_y}\cdot\frac{\partial\boldsymbol{r_i}}{\partial\phi_j}\right)+Q_z\left(\boldsymbol{r_z}\cdot\frac{\partial\boldsymbol{r_i}}{\partial\phi_j}\right)+Q_i\left(\boldsymbol{r_i}\cdot\frac{\partial\boldsymbol{r_i}}{\partial\phi_j}\right)\right] \quad (4)$$

where the operator "sign" yields the first term in parentheses with the sign of the second term and Q_x, Q_y, Q_z, and Q_i are given by:

$$Q_x = 3\Delta\chi_{rh}(\boldsymbol{r_x}\cdot\boldsymbol{r_i})$$
$$Q_y = -3\Delta\chi_{rh}(\boldsymbol{r_y}\cdot\boldsymbol{r_i})$$
$$Q_z = 6\Delta\chi_{ax}(\boldsymbol{r_z}\cdot\boldsymbol{r_i})$$
$$Q_i = -\Delta\chi_{ax}\left[2+\frac{5}{r_i^2}[3(\boldsymbol{r_z}\cdot\boldsymbol{r_i})^2-r_i^2]\right]-\frac{3}{2}\Delta\chi_{rh}\left[\frac{5}{r_i^2}[(\boldsymbol{r_x}\cdot\boldsymbol{r_i})^2-(\boldsymbol{r_y}\cdot\boldsymbol{r_i})^2]\right] \quad (5)$$

and where $\frac{\partial \boldsymbol{r_i}}{\partial \varphi_j}$ is the partial derivative of the vector $\boldsymbol{r_i}$ with respect to the dihedral angle φ_j which moves either atom i with respect to the metal or vice versa (in the latter case the derivative simply changes sign). Further details on the practical implementation of PSEUDIANA are given in Appendix 1.

The common usage of the program DIANA, when solving structures from computer-generated random coil initial structures, is to introduce the constraints in a stepwise fashion according to how far apart in the sequence the residues in question are [31, 32]. In this case, it was possible to run the program PSEUDIANA on the already existing structures [11] by applying all constraints simultaneously. Accordingly, only the last three minimization steps were performed following the standard procedure whereby the total target function is successively evaluated by weighting the atomic Van der Waals radii 0.2, 0.6 and 2.

As already reported [11], the prosthetic group was modeled by constructing a new amino acid, called HES, constituted by a histidine (the axial histidine) and the ferriheme. The residue HES was anchored to the protein by the proximal histidine peptide bonds and by two other links to the thioether sulfurs.

Results and discussion

The chemical shifts of the cyanide derivative of a variant of the oxidized *Saccharomyces cerevisiae* iso-1-cytochrome *c* containing the Met80Ala mutation (Met80Ala cyano-cyt *c*) [11] were compared with the published [35] chemical shifts of the reduced anion-free wild-type species in the same experimental conditions. Protons more than ≈ 1.5 nm from the iron experience the same chemical shifts in the two species within 0.05 ppm. This value was thus taken as the tolerance for the following best-fitting treatment. About 330 signals had a difference in shift larger than 0.05 ppm. Among them, 280 could be used for structural refinement because a safe assignment was available for both oxidized and reduced forms. Thirty-five signals had δ_i^{pc} values smaller than 0.05 ppm, but nevertheless their shifts were used as further constraints. Indeed, experimental δ_i^{pc} values close to zero bear the same information content as large δ_i^{pc} values, in that they impose either a large distance from the paramagnetic center or closeness to the magic angle ($\theta = 54.74°$).

As the goal was that of a safe estimate of the hyperfine pseudocontact shifts, the problem arose of finding an ideal diamagnetic reference. No such ideal reference diamagnetic protein exists, because any diamagnetic reference must be in the reduced state and may well be structurally and electronically different, in some details, from the actual oxidized compound. The difference may be even larger in the present case, due to the additional difference in one axial ligand between the two proteins. However, relaxing the conditions of acceptance of a diamagnetic reference makes the approach described even more general. In this respect, the present δ_i^{pc} uncertainty of 0.05 ppm (30 Hz at 600 MHz) may be considered satisfactory with respect to the goal of refining an available solution structure. In the wild-type protein, the structural differences between oxidized and reduced forms have been proposed to be mainly due to slight movements of the heme and changes in a few hydrogen bonds. This proposal was based on differences – as large as 5 ppm – between calculated and observed pseudocontact shifts [36]. While it is unlikely that these differences are due to variation of the diamagnetic contribution to the observed shift between the reduced and the oxidized proteins, we de-

Table 1 Values of the NOE, pseudocontact shift and total target function ranges in the families of the 17 best structures during the various steps of the refinement procedure. The RMSDs for backbone (*BB*) and all heavy atoms (*HA*) are also reported, together with the average χ tensor anisotropy parameters, for the structures obtained at each step

Step	t^{NOE} (nm^2)	t^{pc} (nm^2)	t^{tot} (nm^2)	RMSD^{BB} (pm)	RMSD^{HA} (pm)	$\Delta\chi_{ax} \pm 3\sigma$ [a] ($m^3 \times 10^{32}$)	$\Delta\chi_{rh} \pm 3\sigma$ [a] ($m^3 \times 10^{32}$)	n_{r_z} [b]	l_{r_x} [b]
0[c]	0.001–0.002	0.234–0.202	0.235–0.217	70	132	2.779 ± 0.020	0.585 ± 0.022	0.9997	0.6803
1	0.008–0.009	0.030–0.037	0.048–0.058	63	126	2.879 ± 0.002	0.585 ± 0.004	0.9999	0.7084
2	0.007–0.009	0.026–0.031	0.043–0.053	63	127	2.957 ± 0.002	0.586 ± 0.004	0.9999	0.7320
3	0.009–0.009	0.026–0.030	0.042–0.049	63	129	3.017 ± 0.003	0.592 ± 0.003	0.9999	0.7424
4	0.008–0.008	0.024–0.027	0.040–0.049	61	126	3.102 ± 0.002	0.599 ± 0.003	1.0000	0.7629
—	—	—	—	—	—	—	—	—	—
17	0.008–0.009	0.022–0.024	0.036–0.042	58	123	3.306 ± 0.001	0.711 ± 0.001	0.9992	0.8088
18	0.008–0.010	0.022–0.024	0.036–0.042	58	124	3.309 ± 0.002	0.705 ± 0.002	0.9993	0.8073
1b[d]	1.392–4.636	0.009–0.023	1.426–4.666	79	137	2.864 ± 0.001	0.596 ± 0.003	0.9999	0.6896

[a] The 3σ values are obtained from the individual χ tensor anisotropy parameters calculated for each of the 17 best structures. They reflect the decrease in RMSD

[b] Only two of the three independent direction cosines are reported, as the almost perfect alignment of r_z along the molecular z axis permits the definition of the r_x and r_y positions in the xy plane using only one positive direction cosine

[c] Calculated after a minimization performed *without* inclusion of the pseudocontact shift constraints

[d] Calculated after a minimization performed *without* inclusion of the NOE constraints

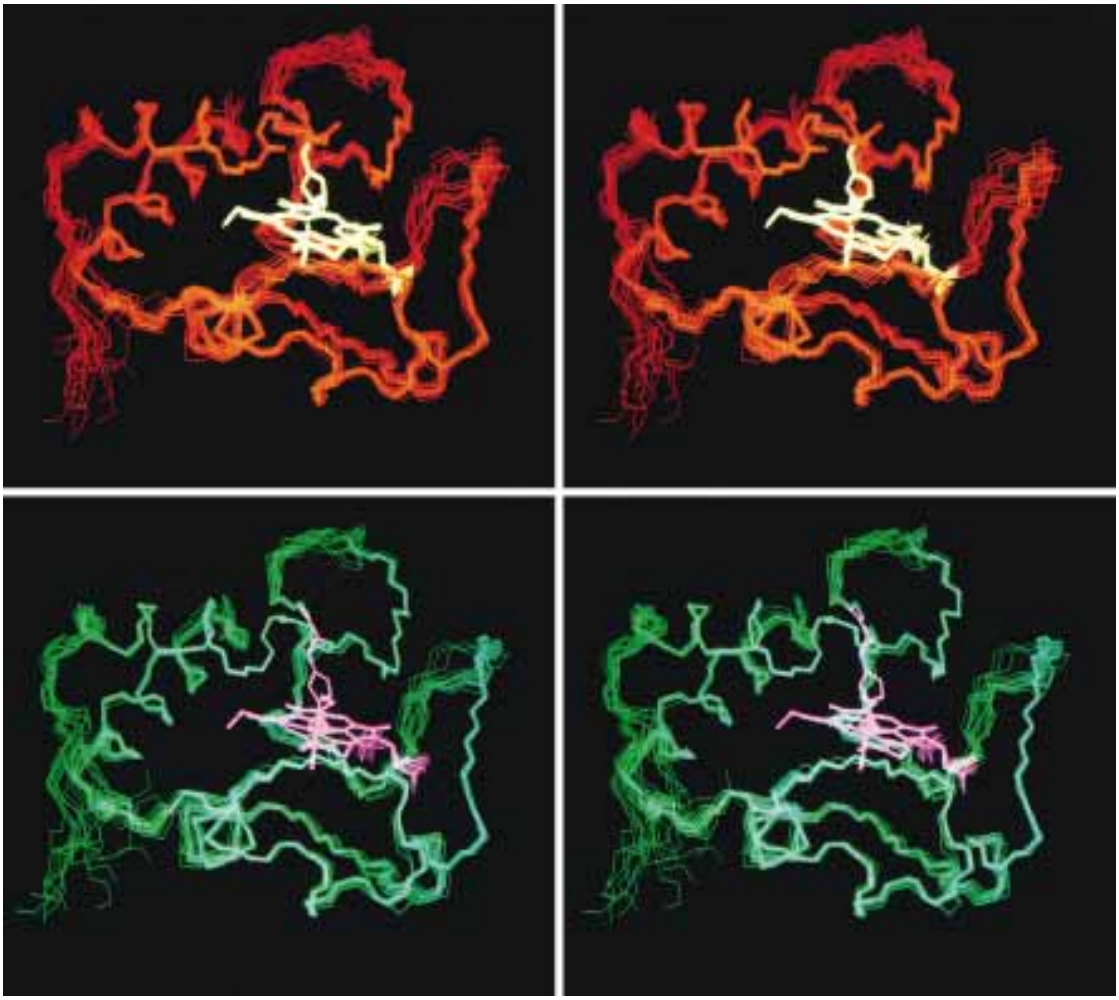

Fig. 2 Comparison between **A** the 17 best structures of the original DIANA family [11] ($RMSD^{BB}$ = 70 pm) and **B** the 17 best structures of the final PSEUDIANA family ($RMSD^{BB}$ = 58 pm). The **A** family corresponds to step 0 in Table 1, while the **B** family corresponds to step 18 in Table 1. The modest atomic displacements from **A** to **B** cause quite significant variations in the $\Delta\chi_{ax}$, $\Delta\chi_{rh}$ and l_r parameters of the χ tensor (Table 1)

cided to address this point by checking the final agreement between calculated and experimental pseudocontact shifts.

Structure refinement

The starting structural model was that corresponding to a family of 17 structures with RMSD for residues 1–102 of 70 pm and 132 pm for the backbone (BB) and all the heavy atoms (HA), respectively, available in the PDB (entry 1FHB) [11] (Fig. 2A). As it is possible from a single structure to determine the five parameters ($\Delta\chi_{ax}$, $\Delta\chi_{rh}$, and three independent direction cosines) that define the magnetic susceptibility tensor anisotropy, the same parameters for an average tensor can also be obtained by finding the best fit using a family of structures. We calculated the average tensor anisotropy from the original extended family of 39 structures [11], from which the 17 best structures had been selected. We chose to use the extended family with the sole aim of having a broader basis set. This holds for the whole procedure to be described. The values of the χ tensor anisotropy parameters are reported as the values at step 0 in Table 1.

The distance geometry (DG) program [31, 32] modified to accept the pseudocontact shifts as further structural constraints as reported in Materials and methods (PSEUDIANA) was used at this point by simultaneously applying the already existing 1426 NOE constraints with the addition of 315 differences in chemical shifts between protons assigned in both the oxidized paramagnetic and in the reduced diamagnetic proteins. Only the final three minimization steps of PSEUDIANA were performed on each member of the original family, with all constraints (NOEs + pseudocontact shifts) included. The availability of starting structures permits this shortcut, which makes the minimization noticeably quicker than the whole DIANA procedure. The latter is used when starting from random structures

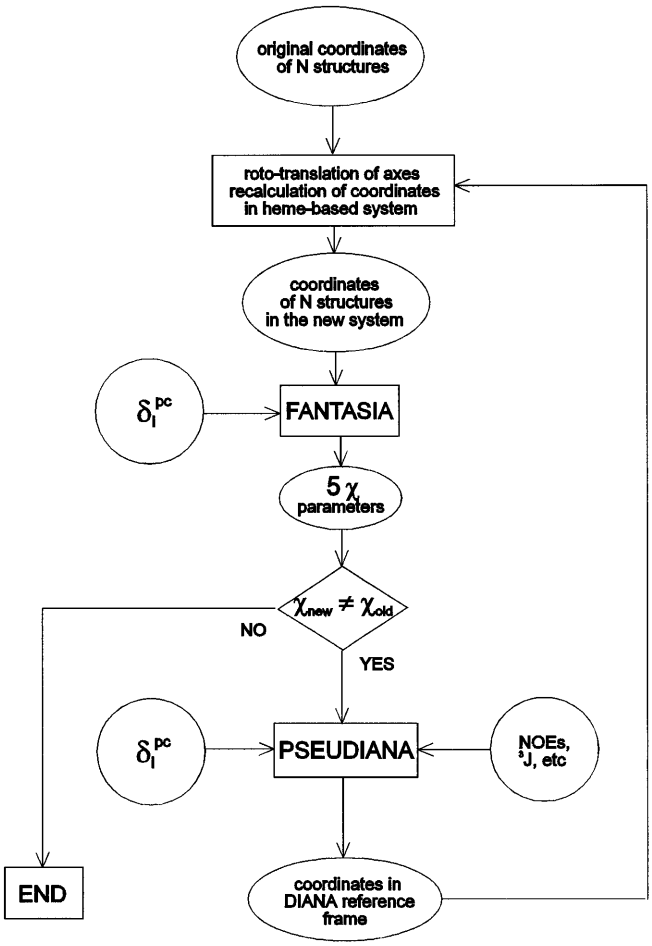

Fig. 3 Flow chart showing the refinement strategy. The coordinates of the starting family of structures are first expressed in the heme-based reference system. The best average χ tensor anisotropy parameters are then calculated from the experimental δ_i^{pc} values. The disagreement between calculated and experimental δ_i^{pc} values, expressed by the target function t^{pc}, is then minimized, together with all other contributions to the total target function, using the program PSEUDIANA, thereby producing a new set of structures. From the coordinates of the latter, expressed again in the heme-based reference system, new average χ tensor anisotropy parameters are calculated. The procedure is repeated until the χ parameters do not vary by more than 1% from the previous step

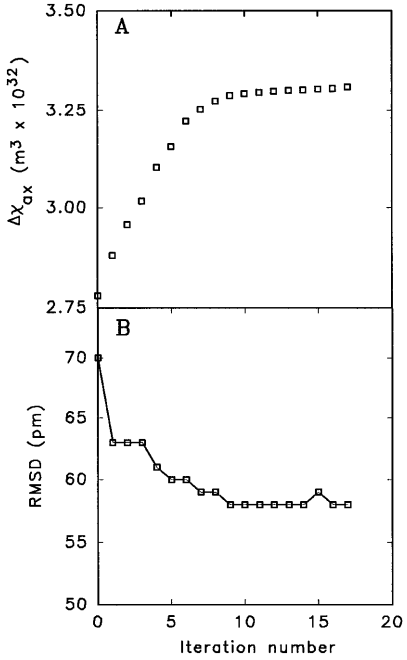

Fig. 4 Progressive variation **A** of $\Delta\chi_{ax}$ (as the most representative of the five parameters defining the χ tensor) and **B** of the $RMSD^{BB}$ values within the 17 best structures along the various minimization steps. The figure illustrates the relatively slow convergence of both $\Delta\chi_{ax}$ and $RMSD^{BB}$ to their self-consistent values, as well as the importance of the self-consistent procedure in achieving a reliable set of χ tensor anisotropy parameters (**A**) and reliable structural refinement (**B**)

and introduces NOE constraints in a stepwise fashion [31, 32] (see Materials and methods).

The 17 structures which had the lowest t^{tot} after minimization had an RMSD of 63 pm for the BB atoms and of 126 pm for all HA (step 1, Table 1). On the other hand, the highest target function had a somewhat higher value than that of the starting family. It increased from 0.002 to 0.009 nm^2 for the NOEs, while the pseudocontact shift component was 0.037 nm^2. The increase in the NOEs' target function was due to the introduction of new constraints and suggested that the calculated structures were not completely consistent with the average χ tensor anisotropy. At this stage, a new average tensor was calculated by fitting to the experimental δ_i^{pc} values the pseudocontact shifts calculated from the new family of structures using the χ tensor anisotropy parameters. The χ parameters at step 1 were somewhat different from those at step 0, indicating that self-consistency had not been achieved.

The whole procedure, summarized in the flow chart of Fig. 3, was then repeated (18 times), until no variation (within 1%) in the values of both $\Delta\chi_{ax}$ and $\Delta\chi_{rh}$ parameters was obtained (Fig. 4, Table 1). The target function maintained a maximum value of 0.010 nm^2 for the NOE constraints, with a maximum contribution due to the pseudocontact shifts of 0.024 nm^2 (step 18, Table 1), while the RMSD values for the 17 best structures decreased to 58 pm for the backbone (Fig. 4, Table 1) and 124 pm for all heavy atoms. The resulting family with improved resolution is shown in Fig. 2B. Comparison of Fig. 5A and Fig. 5B shows the corresponding improvement in the agreement between calculated and experimental δ_i^{pc} values. It can be noted that the uncertainty in the $\Delta\chi_{ax}$ and $\Delta\chi_{rh}$ parameters, estimated from the spreading of the individual tensor parameters for each structure (Table 1), is already very low at step 1, although the parameters themselves keep drifting. Likewise, the agreement between calculated and experimental δ_i^{pc} values is already almost as good as in

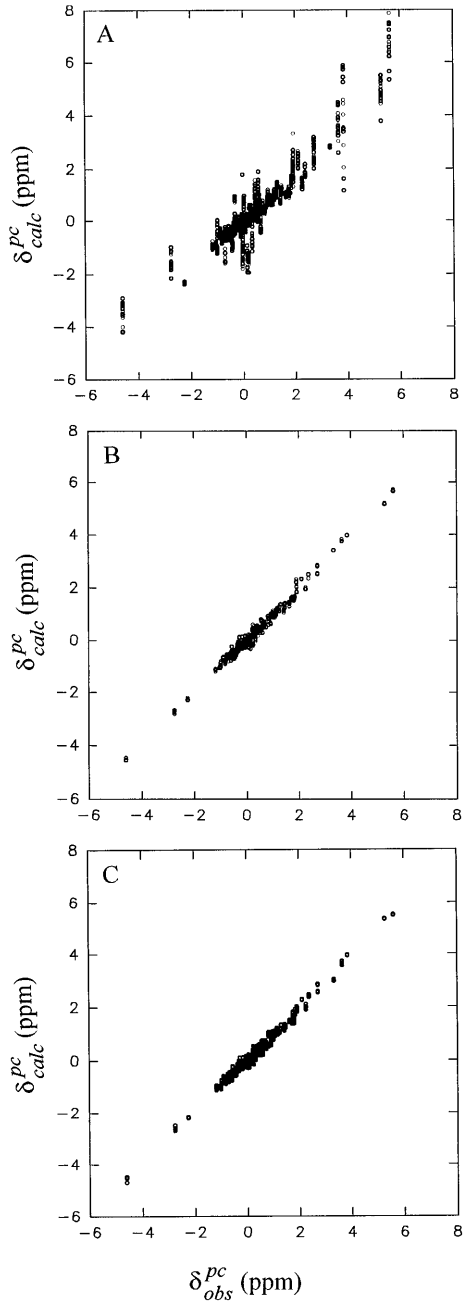

Fig. 5A–C Comparison of $\delta_{calc}{}^{pc}$ vs $\delta_{obs}{}^{pc}$ plots performed at step 0 (**A**) and step 18 (**B**). The visually dramatic improvement in the overall agreement reflects the decrease in the t^{pc} from 0.234 nm^2 at step 0 to 0.022 nm^2 at step 18 (Table 1). **C** The equally dramatic improvement obtained in a single minimization step *without* NOE constraints. However, the high target value for the latter (Table 1, last line) demonstrates that this non-self-consistent procedure is unreliable

Fig. 5B (not shown). This behavior will be discussed further below.

The novelty of the present approach is that the tensor calculated from the pseudocontact shifts and used for structure calculations was refined, together with the atomic coordinates, in the *presence* of the original NOE constraints used for calculating the structure. This is the reason why relatively slow convergence to the final values was observed (Fig. 4 and Table 1). It is instructive to note that when the original structure was refined in the *absence* of the original NOE constraints (step 1b, Table 1), convergence was achieved immediately, t^{pc} dropped to a very low value, and the agreement between calculated and experimental δ_i^{pc} values was very good (Fig. 5C). However, the t^{NOE} value became exceedingly high, the $\Delta\chi$ parameters remained rather similar to those of step 1 in Table 1, and the RMSD values *increased* with respect to the starting structures. In the light of the present results obtained after self-consistent convergence, this means that neither the structure nor the χ tensor anisotropy parameters obtained without the NOE constraints can be considered to constitute adequate refinements of the starting values. As noted above for step 1, the small uncertainty of the χ tensor anisotropy parameters and the good correlation between calculated and experimental δ_i^{pc} values were not, in themselves, reliable indicators of the goodness of the χ anisotropy parameters.

The determinations of χ tensor anisotropy parameters reported in the literature using pseudocontact shifts and a structural model (often represented by the solid state X-ray structure) [17, 21–25] have not included a self-consistent approach and may therefore suffer from relatively large error. Disagreements between calculated and observed pseudocontact shifts can still be, and have been, pinpointed to possible structural differences between the paramagnetic and diamagnetic forms [28, 36] or to inaccuracies of the starting structure [26]. In the latter case [26], the achievement of a refined structure was claimed, but it merely corresponds to our step 1b.

The present self-consistent approach therefore represents a significant step forward in the refinement of a solution structure of a paramagnetic protein. In summary, notable features of this procedure are: (1) The significant decrease in backbone atom RMSD. It is possible that this improvement is due more to the nature than to the number of the new constraints which, due to the r^{-3} rather than the r^{-6} dependence of the NOEs, are long-range constraints with respect to the metal center. This is illustrated in Fig. 6, where the protein residues are color-coded according to the experimental δ_i^{pc} values of their protons, showing how far from the metal center the paramagnetic effect is still observable. (2) The rather uniform distribution of the improvement in the RMSD values per residue (Fig. 7), with some peak values also showing a significant decrease. The use of a large number of almost uniformly distributed pseudocontact shifts, even below the threshold of tolerance, accounts for the uniform distribution of the RMSD improvement. (3) The sizable increase in the values of $\Delta\chi_{ax}$ and $\Delta\chi_{rh}$ ($>20\%$) and the change in orientation of the x and y axes ($>10°$) from the beginning to the end of the self-consistent refinement (Table

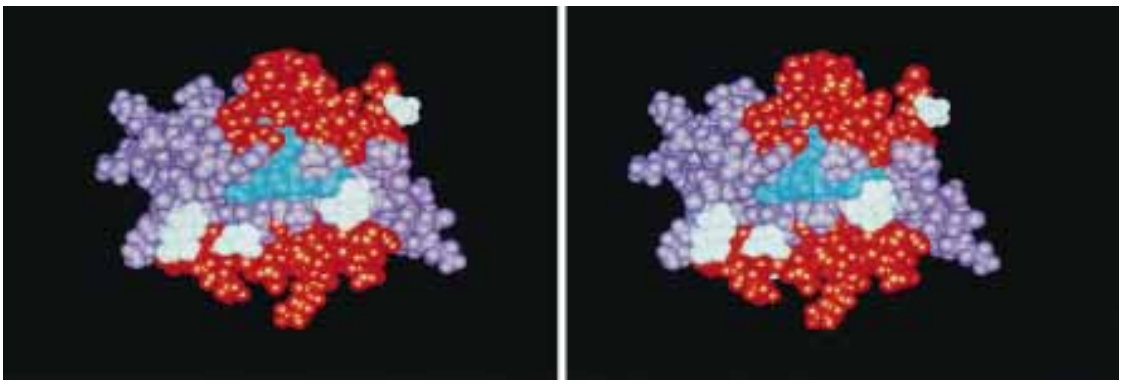

Fig. 6 The most representative refined structure (chosen as the one with the lowest RMSD from the average of the best 17 structures) color-coded to show how far from the metal center sizable δ^{pc} values are observed. Residues having at least one proton with $\delta^{pc} > 0.05$ ppm are colored *orange*, those with at least one proton with $\delta^{pc} < -0.05$ ppm are colored *violet*, and those unassigned or with no proton with $|\delta^{pc}| > 0.05$ ppm are colored *white*. Residues with protons experiencing both upfield and downfield shifts are colored accordingly. The heme, axial histidine and heme-bound cysteines are colored *cyan*: the hyperfine shifts of protons in these groups experience a contact shift contribution and could not be used as constraints. The color coding clearly delineates the dipolar field from the metal, with its familiar d_{z^2} shape. The axial *orange* lobes are regions of downfield shift, and the equatorial *violet* toroid is the region of upfield shifts

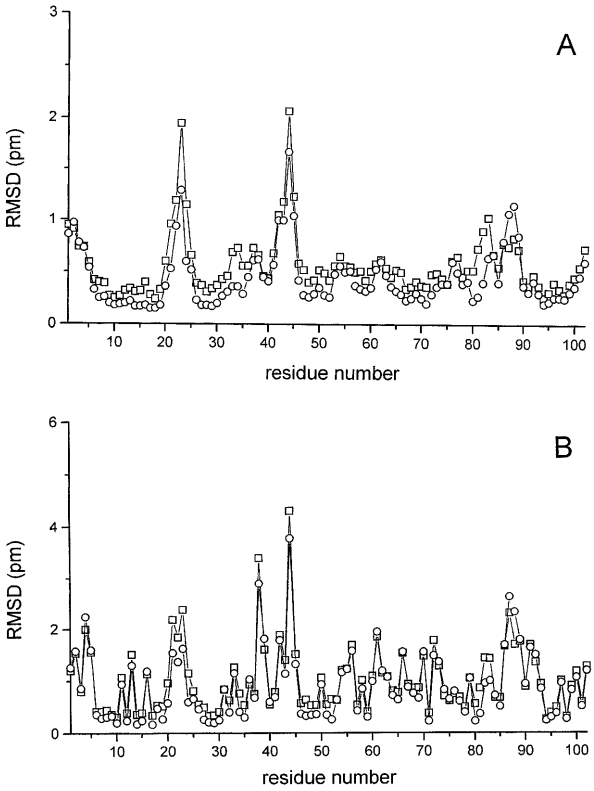

Fig. 7A, B Plot of the RMSD per residue for the 17 original (□) and final (○) best structures. The backbone atom values are shown in **A**, the all heavy atoms values in **B**. It appears that there is a homogeneous decrease in RMSD for most residues, especially for backbone atoms, as well as some improvement in the disordered regions centered around residues 23 and 44

1). These changes again point to the low reliability of the estimates of the tensor parameters, if the starting structure differs somewhat from the true one. At this point, a careful analysis of the violations in NOEs and pseudocontact shifts for each residue showed that, within the final family of structures (step 18), there were no consistent NOE violations larger than 4 pm and no consistent pseudocontact shift violations larger than 0.45 ppm. Furthermore, there were no regions of the structure with appreciable clustering of consistent violations. This analysis gives us confidence that the quality of the results is good and that errors in the evaluation of the diamagnetic reference are overcome by the self-consistent procedure.

The final family of structures was narrower than the original set but still within its range of uncertainty. The RMSD between the average structures of the original set of structures and of the refined family was 67 pm for the backbone.

χ tensor and contact shifts

The determination of the χ tensor anisotropy and of its principal axes allowed us to determine the contact shifts of the hyperfine-coupled protons by factoring out the pseudo-contact contributions. This was possible under the assumption that the unpaired electron was located on the metal ion. This assumption was reasonable for protons that do not bear any spin density capable of dipolar interactions. The results are reported in Table 2. The contact shift patterns of the porphyrin ring methyl protons, which, at variance with the α propionate and thioether protons, were not affected by their dihedral angle with the heme carbon p_z orbital, are in qualitative agreement with theoretical predictions [43]. In fact, for the present histidine orientation, the histidine nitrogen p_π orbital lies approximately parallel to the β meso–δ meso direction, and the smallest spin density is expected on 3-CH_3. The present example joins other cyanide adducts of heme proteins (Table 2) showing a

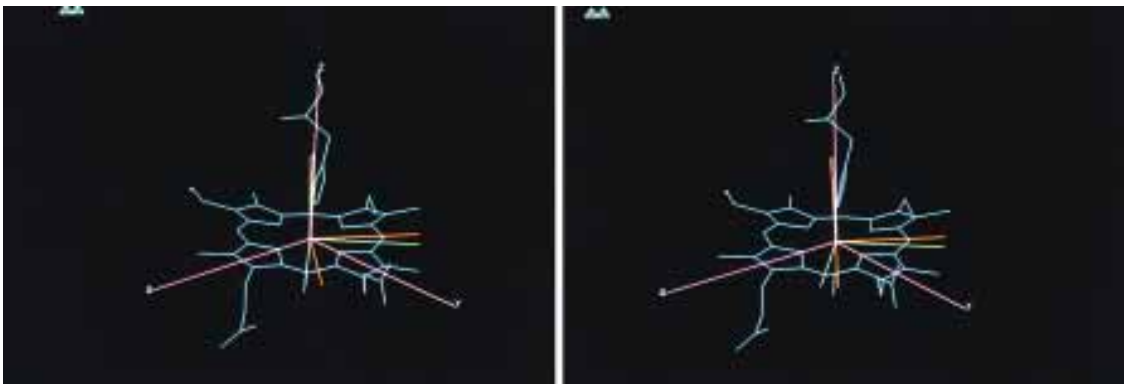

Fig. 8 Orientation of the χ tensor axes with respect to the heme-based coordinate system (*pink*) at steps 0 (*green*) and 18 (*orange*) (Table 1). The χ_{xx} green and orange axes point outward, approximately in the direction of the γ meso carbon. The χ_{xx} axis of step 18 is almost coincident with the projection of the axial histidine ring on the heme plane

variety of His p_π orientations and all in qualitative agreement with predictions.

The contact shifts of the axial histidine ortho-like protons were negative, the H 1 being much larger in absolute value than Hδ2. Negative contact shifts, in the same order, were also observed for the axial histidine ortho-like protons in the other cases reported in Table 2, the present system showing the largest difference.

As to the principal directions of the χ tensor, the z axis is perpendicular to the average heme plane within the experimental error (Fig. 8). This appears also to be the case in the cyanide adduct of lignin peroxidase (LiP) but not in those of myoglobin (Mb) and horseradish peroxidase (HRP). The x and y directions in Met80Ala cyano-cyt c were almost exactly along and perpendicular to the projection of the histidine ring plane on the xy plane. This is similar to what has been found in HRP and Mb, in spite of the fact that in the latter two cases the His Np_π is essentially along the pyrrole nitrogens direction (pyrroles II/IV in HRP and pyrroles I/III in Mb). In contrast, in LiP the χ tensor axes do not show any obvious relation with the His ring projection on the heme plane, although the histidine ring has an orientation at approximately 90° from that in Met80Ala cyano-cyt c and therefore can be considered homologous to the latter except for an interchange of the x and y axes. It has been recently suggested that ^{13}C-NMR data may be capable of shedding further light on this problem [44].

Conclusions

While it was already known that the δ_i^{pc} values can be used to obtain structural information in solution, they were used here for the first time in conjunction with NOE constraints to obtain a family of structures or to refine a structure already available from NOE constraints. This procedure showed that the evaluation of the anisotropy and direction of the magnetic susceptibility tensor can be affected by significant errors if the starting solution structure is not accurate. Whereas here self-consistency with the NOEs is sought, and represents a check, no evaluation of the error is possible when the starting structure is that of the solid state structure of the same protein or, worse, of a homologous one. In other words, the best procedure to obtain the magnetic susceptibility tensor anisotropy and to factor out the hyperfine shifts is the present one, based on the simultaneous analysis of solution NMR constraints and pseudocontact shifts. The precise determination of the χ anisotropies and of their directions is a source of fruitful information on the electronic structure of the metal ion and the coordination polyhedron.

The refined structure had a resolution substantially higher than that based only on NOEs, although the violations of the NOE constraints increased somewhat. This was not a serious problem as long as t^{NOE} re-

Table 2 Calculated contact shifts for heme methyl and proximal histidine resonances in the cyanide adducts of some heme proteins. The angle α between the histidine p_π and the heme-based x axis is also reported

Signal	Met80Ala cyano-cyt *c*	δ^{con} (ppm)		
		LiP[a]	HRP[b]	Mb[c]
Heme				
1-CH_3	16.9	2.7	2.8	18.4
3-CH_3	10.5	30.5	24.9	6.7
5-CH_3	20.8	5.5	6.6	27.8
8-CH_3	24.6	17.7	28.7	15.8
Proximal His				
Hδ2	− 1.8	−10.5	−16	− 6.2
H 1	−31.4	−34.2	−20	−15.8
α (deg)	139	53	75[d]	8

[a] Taken from [37]
[b] Estimated from [38, 39] as reported in [37]
[c] Taken from [22]
[d] Measured using the cytochrome *c* peroxidase X-ray structure as a model [40–42]

mained $\leq 0.010\ nm^2$ [31, 32]; in any case, our approach based on DIANA used only a semiquantitative calibration procedure [31, 32].

In the present research the pseudocontact shifts were used to refine an existing structure. If one had an idea of the tensor from independent methods, e.g. from ^{13}C-NMR data of the heme methyls [44, 45], this very same approach could be used right from the beginning of the structure determination. Use of the program from scratch is possible and may be appropriate when the system provides a low number of NOEs.

A general problem which requires further comment is the choice of the diamagnetic reference for the determination of the pseudocontact shifts. The use of the shifts of the diamagnetic analogue relies on the assumption that it is structurally equal to the paramagnetic system. This assumption may be verified a posteriori. If some input data are not consistent with the final output, they can be omitted and their inconsistency should be analyzed. Alternatively, one could use only the larger pseudocontact shifts with a larger tolerance. In this case the diamagnetic reference could be calculated from available statistics and equations [46–48]. Indeed, the procedure is rather flexible and can be varied according to personal taste and the specific goals of the research.

Finally, one should reflect on the r^{-3} nature of the pseudocontact shifts as compared to the r^{-6} nature of the NOEs. The two contributions average differently in the presence of mobility, and the comparison of NOE or shift violations could be informative.

Acknowledgements This work was supported by CNR, Comitato Scienze Agrarie, Comitato Biotecnologie e Biostrumentazione, and Progetto Strategico Biotecnologie.

Appendix 1

The practical implementation of Eq. 2 in the DIANA program requires several steps. To the HES amino acid, six pseudoatoms, named PX, PY, PZ and AX, AY, AZ and located at unit distance from the iron, are added. They represent, respectively, the x, y and z axis of the heme-based reference system defined above and the axes of the χ tensor expressed by the unit vectors $\boldsymbol{r}_x$, $\boldsymbol{r}_y$, and $\boldsymbol{r}_z$ (Fig. 1). The latter were provided by the program FANTASIA as a set of nine direction cosines of AX, AY and AZ in the PX, PY, PZ system. This allowed us to obtain the positions of the AX, AY, AZ pseudoatoms in the DIANA coordinate frame whatever the position of the PX, PY, PZ pseudoatoms in this system. In this way, the algorithm could be implemented by exploiting the DIANA arrays CX(), CY(), and CZ() which, after each call to the DIANA subroutine GENER [31, 32], contained the new atomic coordinates at that stage of the calculation.

The evaluation of the $\frac{\partial \boldsymbol{r}_i}{\partial \phi_j}$ contributions to the gradient in Eq. 4 was performed, in the coordinate frame of DIANA, indicated by primes, as follows:

$$\frac{\partial \boldsymbol{r}_i}{\partial \phi_j} = \frac{\partial (\boldsymbol{r}'_i - \boldsymbol{r}'_{Fe})}{\partial \phi_j} = \pm \frac{\partial \boldsymbol{r}'_i}{\partial \phi_j} = \pm \boldsymbol{e}'_j \wedge (\boldsymbol{r}'_i - \boldsymbol{r}^{\circ}_j) \qquad \text{(A1)}$$

where $\boldsymbol{e}'_j$ is a unit vector lying on the central bond of the dihedral angle φ_j and oriented toward the moving part of the molecule [49, 50] and $\boldsymbol{r}'_j$ is the position vector of the third atom involved in the dihedral angle.

References

1. Bertini I, Turano P, Vila AJ (1993) Chem Rev 93:2833–2932
2. Banci L, Bertini I, Luchinat C (1994) In: James TL, Oppenheimer NJ (eds) Methods in enzymology. Academic Press, London, pp 485–514
3. La Mar, GN, de Ropp, JS (1993) In: Berliner LJ, Reuben J (eds) Biological magnetic resonance, vol 12. Plenum Press, New York, pp 1–78
4. Luchinat C, Piccioli M (1995) In: La Mar GN (ed) Nuclear magnetic resonance of paramagnetic macromolecules. (NATO ASI Series). Kluwer Academic, Dordrecht, pp 1–20
5. La Mar GN, Chen Z, de Ropp JS (1995) In: La Mar GN (ed) Nuclear magnetic resonance of paramagnetic macromolecules. (NATO ASI Series). Kluwer Academic, Dordrecht, pp 55–74
6. Banci L, Bertini I, Eltis LD, Felli IC, Kastrau DHW, Luchinat C, Piccioli M, Pierattelli R, Smith M (1994) Eur J Biochem 225:715–725
7. Banci L, Bertini I, Dikiy A, Kastrau DHW, Luchinat C, Sompornpisut P (1995) Biochemistry 34:206–219
8. Bertini I, Dikiy A, Kastrau DHW, Luchinat C, Sompornpisut P (1995) Biochemistry 34:9851–9858
9. Bertini I, Eltis LD, Felli IC, Kastrau DHW, Luchinat C, Piccioli M (1995) Chem Eur J (in press)
10. Bertini I, Donaire A, Feinberg BA, Luchinat C, Piccioli M, Yuan H (1995) Eur J Biochem 232:192–205
11. Banci L, Bertini I, Bren KL, Gray HB, Sompornpisut P, Turano P (1995) Biochemistry 34:11385–11398
12. Banci L, Pierattelli R (1995) In: La Mar GN (ed) Nuclear magnetic resonance of paramagnetic macromolecules. (NATO ASI Series). Kluwer Academic, Dordrecht, pp 281–296
13. Ascenso JR, Xavier AV (1983) In: Sinha S (ed) Systematic properties of lanthanides. Reidel, Dordrecht, pp 501
14. Barry CD, North ACT, Glasel JA, Williams RJP, Xavier AV (1971) Nature 232:236–245
15. Barry CD, Glasel JA, Williams RJP, Xavier AV (1974) J Mol Biol 84:471–490
16. Dobson CM, Williams RJP, Xavier AV (1973) J Chem Soc Dalton Trans 2662
17. Campbell ID, Dobson CM, Williams RJP, Xavier AV (1973) Ann NY Acad Sci 222:163
18. La Mar GN, Horrocks Jr. WD, Holm RH (eds) (1973) NMR of paramagnetic molecules. Academic Press, New York
19. Bertini I, Luchinat C (1986) NMR of paramagnetic molecules in biological systems. Benjamin/Cummings, Menlo Park, California
20. Bertini I, Turano P (1994) In: La Mar GN (ed) Nuclear magnetic resonance of paramagnetic macromolecules. (NATO ASI Series). Kluwer Academic, Dordrecht, pp 29–54
21. Lee L, Sykes BD (1983) Biochemistry 22:4366–4373

22. Emerson SD, La Mar GN (1990) Biochemistry 29:1556–1566
23. Bertini I, Luchinat C, Piccioli M, Vicens Oliver M, Viezzoli MS (1991) Eur Biophys J 20:269–279
24. Banci L, Dugad LB, La Mar GN, Keating KA, Luchinat C, Pierattelli R (1992) Biophys J 63:530–543
25. Capozzi F, Cremonini MA, Luchinat C, Sola M (1993) Magn Reson Chem 31:S118–S127
26. Gochin M, Roder H (1995) Protein Sci 4:296–305
27. Sherry AD, Pascual E (1977) J Am Chem Soc 99:5871–5879
28. Turner DL, Williams RJP (1993) Eur J Biochem 211:555–562
29. Lisowski J, Sessler JL, Lynch V, Mody TD (1995) J Am Chem Soc 117:2273–2285
30. Nelder JA, Mead R (1965) Comput J 7:308
31. Güntert P, Braun W, Wüthrich K (1991) J Mol Biol 217:517–530
32. Güntert P, Wüthrich K (1991) J Biomol NMR 1:447–456
33. Hestenes MR, Stiefel E (1952) J Res Natl Bureau Standards 49:409–436
34. Fletcher R, Reeves CM (1964) Comput J 7:149–154
35. Gao Y, Boyd J, Williams RJP, Pielak GJ (1990) Biochemistry 29:6994–7003
36. Gao Y, Boyd J, Pielak GJ, Williams RJP (1991) Biochemistry 30:1928–1934
37. Banci L, Bertini I, Pierattelli R, Tien M, Vila AJ (1995) J Am Chem Soc 117:8659–8667
38. La Mar GN, Chen ZG, Vyas K, McPherson AD (1995) J Am Chem Soc 117:411–419
39. Thanabal V, de Ropp JS, La Mar GN (1987) J Am Chem Soc 109:265–272
40. Poulos TL, Kraut J (1980) J Biol Chem 255:8199–8205
41. Finzel BC, Poulos TL, Kraut J (1984) J Biol Chem 259:13027–13036
42. Edwards SL, Poulos TL (1990) J Biol Chem 265:2588
43. Walker FA (1980) J Am Chem Soc 102:3254–3256
44. Turner DL (1995) Eur J Biochem 227:829–837
45. Banci L, Pierattelli R, Turner DL (1995) Eur J Biochem 232:522–527
46. Giessner-Prettre C, Pullman B (1987) Q Rev Biophys 20:113–172
47. Haigh CW, Mallion RB (1980) Prog NMR Spectrosc 13:303–344
48. Ösapay K, Case DA (1991) J Am Chem Soc 113:9436–9444
49. Abe H, Braun W, Noguti T, Go N (1984) Comput Chem 8:239–247
50. Noguti T, Go N (1983) J Phys Soc Japan 52:3685–3690